

Cite this article: M. Singh, Green synthesis of ZnO nanoparticles using vegetable extracts and their characterization, *RP Cur. Tr. Eng. Tech.* 3 (2024) 61–67.

Original Research Article

Green synthesis of ZnO nanoparticles using vegetable extracts and their characterization

Manjeet Singh*

Department of Physics, Government College Matanhail, Jhajjar – 124106, Haryana, India

*Corresponding author, E-mail: manjeetgur@gmail.com

ARTICLE HISTORY

Received: 18 Sept. 2024

Revised: 05 Nov. 2024

Accepted: 08 Nov. 2024

Published online: 12 Nov. 2024

KEYWORDS

Green synthesis; ZnO nanoparticles; Vegetable extracts; Fourier transform infrared; X-ray diffraction; Scanning electron microscopy; UV-vis spectroscopy.

ABSTRACT

The synthesis of zinc oxide nanoparticles (ZnO NPs) using various vegetable extracts (onion, cabbage, carrot, and tomato) was carried out in this study. Using Fourier transform infrared (FTIR), X-ray diffraction (XRD), scanning electron microscopy (SEM), and UV-visible spectroscopy, fresh extracted ZnO NPs from onions, cabbage, carrots, and tomatoes are analyzed. According to FTIR results, ZnO NPs containing a few additional functional groups were detected in the 626 cm^{-1} to 1219 cm^{-1} spectrum. XRD measurements showed that ZnO NPs have a Wurtzite hexagonal structure. Furthermore, using Scherrer's equation, ZnO NPs were divided into nanoscales of 17 nm, 18 nm, 24 nm, and 15 nm. SEM images showed almost spherical morphologies for the extraction of onions and tomatoes, and rods and tubes for the extraction of carrots and cabbages, respectively. For every extract, the UV-vis spectroscopy data showed two sharp peaks. ZnO NP material can be used in metal oxide semiconductor-based systems, as evidenced by the detection of a broad range of energy bandgaps in the 3–4 eV regime. After the successful synthesis of the dye-sensitive solar cell based on ZnO NPs, the device's efficiency was assessed by monitoring the current density-voltage behavior in the presence of artificial sunshine. Using the greenly synthesized ZnO NPs to manufacture dye-sensitive solar cells is an easy and practical solution to improve our future.

1. Introduction

Power can come from a variety of sources, from ancient fires created by burning forests to modern electrical industries. Its use is one of the most important parts of human contact in daily life. However, the increase in industrial development in many nations has resulted in indicators of insufficiency in the fundamental energy resources that humans used for reaping. As a result, rising worries about the energy crisis, global warming, the depletion of fossil resources, and environmental issues are motivating research efforts to develop sustainable, inexpensive, and clean energy sources that will power the globe going forward [1]. Metallic oxide semiconductor (MOS) nanostructures are used for reliability in the most recent developments in solar energy transformation technologies that employ bio-semiconductors as the light harvesting layer. According to the National Renewable Energy Laboratory, charge extraction and transit involve both the electrode and the biomolecules [2]. The study and application of materials at the nanoscale is the focus of the broad field of nanoscience. It is growing in popularity. Because of changes in their properties, including form size, size distribution, and a stronger measure of the ratio between surface area and volume, nanoparticles (NPs) exhibit new and improved attributes as compared to their bulk counterparts [3]. The unique electrical, mechanical, optical, and magnetic properties of metal NPs have led to a broad spectrum of applications in research and innovation in recent years [1–3]. Zinc oxide nanoparticles (ZnO NPs) have attracted a lot of attention from researchers in recent years due to its essential uses as antibacterial agents, photovoltaic cells, textile textiles, and polymers to destroy microbes [3].

In order to address the demand for environmentally acceptable energy sources, nanomaterials have been the subject of much research. One area of technology that examines a variety of materials at the nanometric level is called nanotechnology. Electronic engineering, engineering, and materials science are among the fields where its uses might be found. Numerous magnetic and optoelectronic characteristics of nanoparticles are controlled by their composition, size, and shape distribution. The manufacture of nanoparticles using vegetable extract is growing in popularity since it does not require hazardous chemicals and is simple and environmentally friendly [3–5]. Zinc oxide (ZnO) is utilized in this application because to its special properties and strong excitonic binding energy [1–5].

Numerous techniques, such as hydrothermal, solvothermal, sol-gel, direct oxidation, chemical vapour deposition (CVD), electrodeposition (ED), sonochemical, chemical bath deposition (CBD), microwave, and others, can be used to regularly synthesize ZnO NPs [5]. Conversely, these methods are costly, risky, and environmentally unfriendly. The need for synthesizing ZnO with high yields, low cost, and non-toxicity through the use of biological sources and ecologically friendly exploration and synthesis techniques is increasing these days. Environmentally friendly resources, such as plant extracts (leaf, flower, bark, root, seed, and peel), as well as bacteria, fungus, and enzymes, are utilized to synthesize zinc oxide nanoparticles [6]. Since vegetable removal is widely available and reasonably priced, it was used in this study. ZnO NPs have been found to be synthesized from a variety of vegetable



extracts [6–8]. In their studies, various researchers have reported the use of ZnO NPs in the manufacturing of dye-sensitive solar cells. No research has been done on the green synthesis of zinc oxide nanoparticles using tomatoes, onions, cabbage, and carrots as a resource for dye-sensitive solar cell implementation, nor have any comparisons been made between them. The green synthesis technique is used in this study to synthesize ZnO NPs, and in addition to ZnO, preparations of tomato, onion, cabbage, and carrot are used as stabilizing and reducing agents. A range of methods, such as Fourier transform infrared, X-ray diffraction, scanning electron microscopy, and an ultraviolet/visible spectroscope, were used to evaluate the synthesized NPs. The synthesis and analysis of ZnO NPs based on onion and cabbage extracts is one of the goals of this study. Another is to investigate the application of ZnO NPs in the fabrication of dye-sensitive solar cells using tomato and carrot extracts.

2. Experimental

2.1 Synthesis methods

We purchased fresh tomatoes, carrots, onions, and cabbage in a market. Additionally, ethanol (99.5%) and zinc acetate dihydrates (99.7%) were purchased from the market. First, distilled water was used to rinse the tomato, onion, cabbage, and carrot four times before they were cut into small slices. After weighing and blending the tomato, onion, cabbage, and carrot into the distilled water, the procedure was carried out four more times. After combining 25 grams of onion powder, 35 grams of cabbage powder, 25 grams of carrot powder, and 25 grams of tomato powder with 250 milliliters of distilled water in different beakers, the solutions were brought to a boil for 25 minutes at a time to produce aqueous extracts. After being frozen, the mixtures were filtered using a paper and stored at 40°C until they were required for a subsequent use. ZnO NPs' green syntheses were carried out following established protocols [9]. 20 g of $\text{Zn}(\text{CH}_3\text{COO})_2 \cdot 2\text{H}_2\text{O}$ was dissolved in 1 liter of distilled water using sonication to produce a 2M concentration of zinc acetate dehydrate $\text{Zn}(\text{CH}_3\text{COO})_2 \cdot 2\text{H}_2\text{O}$ in a beaker. Until it was required, the mixture was kept in the refrigerator. Onion (15 mL), tomato (15 mL), cabbage (15 mL), and carrot (15 mL) preparations were mixed with a 15 mL $\text{Zn}(\text{CH}_3\text{COO})_2 \cdot 2\text{H}_2\text{O}$ solution in a beaker with a stirrer for 15 minutes. The mixture was then let to stand at room temperature for 20 hours prior to testing. As the color changed from white to light brown to dark brown over time, the decline of Zn-ion was seen as a gradual color shift from white to pale brown to brown. The synthesis of ZnO NPs had been causing the mixture's texture to change. Before being used, the generated nanoparticles were rinsed six times with ethanol and distilled water and spun at 10,000 rpm for 20 minutes during the course of the next day. After the samples were collected, they were transferred to a Petri plate and vacuum-oven dried for 10 hours at 65°C.

2.2 Characterization techniques

FTIR Analysis

Using a scanning spectrum of 4000–400 cm^{-1} and a resolution of 5 cm^{-1} , the PerkinElmer FTIR Spectrum One was utilized to analyze and characterize the connected functional groups to the exterior of the synthesized ZnO NPs in order to study and characterize their surface. The specimen was regularly and suitably combined with solid KBr for both FTIR analyses. The KBr was then squeezed to form an incredibly

thin layer, which was employed for the FTIR analysis and kept in the instrument's scanning chamber.

X-Ray Diffraction and SEM Analysis

Using an X'Pert Pro X-ray diffractometer that generated Cu K α radiation (with an angular resolution of 1.55 Å), the X-ray diffraction (XRD) distribution of ZnO NPs was obtained. The crystalline particle sizes that have been generated are being assessed using it. A small amount of the powder sample was used for characterization. X-ray generators were operating at 45 kV and 25 mA of current to the target at room temperature. At room temperature, temperature-dependent strengths were measured in increments of 0.01 throughout a temperature range of 100 to 800°C. The diffractometer was connected to a computer for data collecting and characterization displays. By contrasting the crystal's peak locations with those of the already available standard data, the structure of the crystal had to be verified. Before being moved to a metal plate, roughly 0.6 g of the generated ZnO NPs were crushed into fine powders for each sample and measured with a beam balance. Following the formation of the NPs, the morphology of the particles was investigated using a scanning electron microscope (Hitachi, H-7600), which functions under high vacuum and has spatial resolutions of 50 to 100 nm and magnifications ranging from 20x to roughly 30,000x. For ZnO NPs with fixed diameters, a greater magnification was achieved by reducing the sample's raster width and vice versa. The absorbance spectra of the synthesized ZnO NPs were measured using UV-vis spectroscopy (Perkin Elmer LAMBDA 950) operating over a wavelength range of 200–500 nm in a quartz cuvette with a diameter of 1 cm. To produce their solutions, about 0.5 g of ZnO NPs were combined with double-distilled water and then put into a quartz cuvette. The cuvette was then put in an ultraviolet visible spectrophotometer to measure the ZnO NPs' absorption spectra.

3. Results and discussion

3.1 FTIR analysis

A Fourier transform infrared spectral analysis (FTIR) was used to determine the likely functional groups in biomolecules that contain a natural extract and are caused by the reduction of the zinc ion into ZnO NPs.

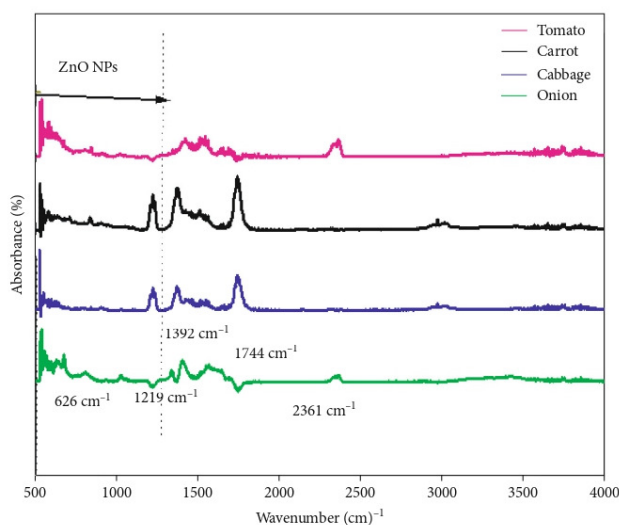


Figure 1: FTIR spectra of ZnO NPs isolated from tomatoes, onions, cabbage, and carrots using green synthesis techniques.

Figure 1 shows the FTIR spectra of the ZnO NPs that were synthesized using vegetable extracts. ZnO NPs synthesized using extracts of onions, cabbage, carrots, and tomatoes showed nearly identical absorption peaks at 626, 1219, 1392, 1744, and 2361 cm^{-1} in their FTIR spectra. Because of the strong and wide peak at 1500-2000 cm^{-1} , which represents the N-H, O-H, and H-bonded phenols and alcohols stretching vibrations of amide groups, respectively, the N-H, O-H, and H-bonded phenols and alcohols stretching oscillations of amide groups are depicted. The bands that appear about 2361 cm^{-1} are indicative of the C-O stretch oscillations. The synthesis of ZnO NPs is indicated by the emergence of a band in the spectra in the 626 cm^{-1} to 1219 cm^{-1} ranges, and the results are in good agreement with the literature [10–12].

3.2 X-ray diffraction analysis

Figure 2 displays the XRD pattern of ZnO NPs that were synthesized using vegetable extracts.

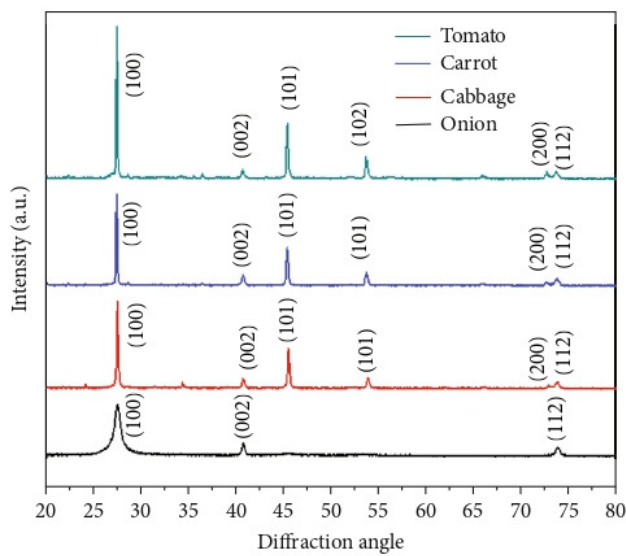


Figure 2: The extracted ZnO NPs isolated from tomato, onion, cabbage, and carrot were subjected to XRD spectrum analysis.

All of the ZnO NPs' XRD diffraction profiles, as reported in the retrieved products [10, 12, 13], are in excellent agreement with the hexagonal wurtzite architecture (hexagonal phase, space group P63mc), which has lattice parameters of $a = b = 3:249$ and $c = 5:206$, in accordance with JCPDS card no. 36-1451. Two large diffraction peaks with corresponding crystal planes of (100) and (002) were seen at 27.39° and 40.64°, respectively. Here, there are just two large peaks visible in the onion-extracted NPs. Furthermore, with the exception of the onion sample, all extracted samples showed 47.31°, 53.60°, 72.63°, and 73.75° with (101), (102), (200), and (112) of crystal planes, respectively. The highest intensity peak was found at (100), indicating the favored growth plane and proving the high purity of ZnO NPs. The trend depicted in Figure 2 is inconsistent with the XRD pattern of green synthesized ZnO NPs reported in the literature [14]. As a result, ZnO NP production was confirmed by XRD. The following Scherrer's equation was used to help determine the nanoparticles' dimensions.

$$t = \frac{0.9\lambda}{\beta \cos \theta} \quad (1)$$

where β is the full width half peak in radians, θ is the degree of diffraction, t is the average size of NPs, and λ is the radiation frequency [12–14].

NPs with mean diameters of 17 nm, 18 nm, 24 nm, and 15 nm have been synthesized using preparations of onions, cabbage, carrots, and tomatoes, respectively. Table 1 shows the average diameters of NPs made using extracts of tomatoes, onions, cabbage, and carrots. The aforementioned results suggest that smaller NPs are produced during the tomato extract instance.

Table 1: Average particle size, FWHM, and diffraction angle of tomato, onion, cabbage, and carrot that were separated from the ZnO NPs.

Extracted samples	2 theta	FWHM (β)	Average particle size (t)
Onion	40.64	0.07345	17.10
Cabbage	40.64	0.05325	18.20
Carrot	40.64	0.04687	24.20
Tomato	40.64	0.08767	15.20

3.3 SEM analysis

The SEM morphology of the isolated ZnO NPs extracted by tomato, onion, cabbage, and carrot, respectively, is shown in Figure 3. In the case of tomato and onion extractions, SEM images show the spherical surface shape, whereas carrot and cabbage are used to synthesize almost nanorods and nanotubes, respectively.

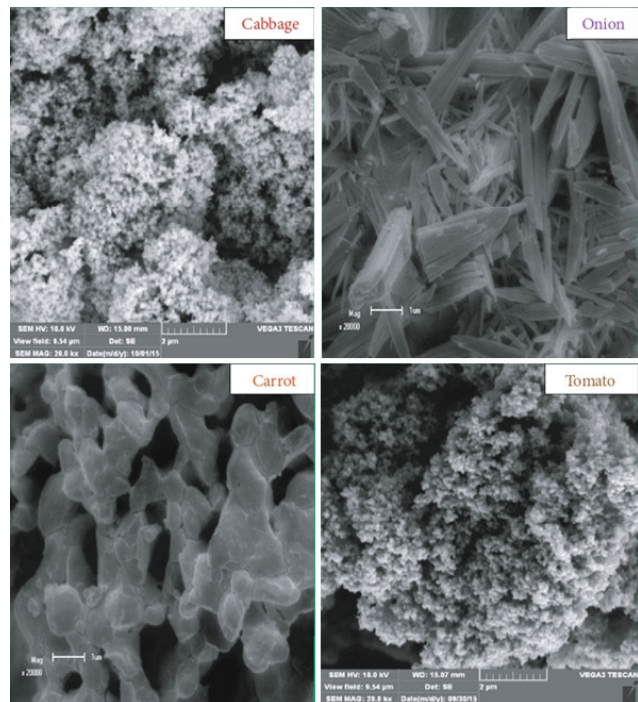


Figure 3: SEM pictures of the ZnO NPs that were extracted using green synthesis techniques from tomatoes, onions, cabbage, and carrots.

The green synthesized structures exhibit uniformity and minimal aggregation due to their modest size. To reduce agglomeration, plant extract functions as both a capping and reducing agent, eliminating the need for expensive and hazardous capping chemicals. Compared to other techniques of synthesizing ZnO NPs, this technique is therefore more economical and environmentally friendly. The synthesized

ZnO NPs' narrow assimilation SEM picture in tomato and onion extracts shows the wurtzite hexagonal structure in detail, with their neighboring contacting surfaces having distinct forms and being smooth [15–18].

UV-vis spectroscopy was used to examine the optical bandwidth of the synthesized ZnO NPs [16, 18]. The synthesized ZnO NPs were uniformly dispersed throughout the triple-filtered water using an ultrasonicator for 5 minutes in order to produce a homogenous solution. Figure 4 displays the UV-visible spectrum of the green synthesized ZnO NPs that were extracted from tomato, onion, cabbage, and carrot. For onion derived NPs, the spectra shows a broad absorption peak at 276 nm and 375 nm. Additionally, ZnO NPs derived from tomatoes, carrots, and cabbage has wavelengths of 215 nm and 343 nm, 214 nm and 310 nm, and 217 nm and 338 nm, respectively. The surface plasmon absorption properties of ZnO NPs are responsible for these peaks. The cumulative oscillation of the open conduction band electrons causes a phenomena when electromagnetic waves affect the surface plasmon absorption [17, 18].

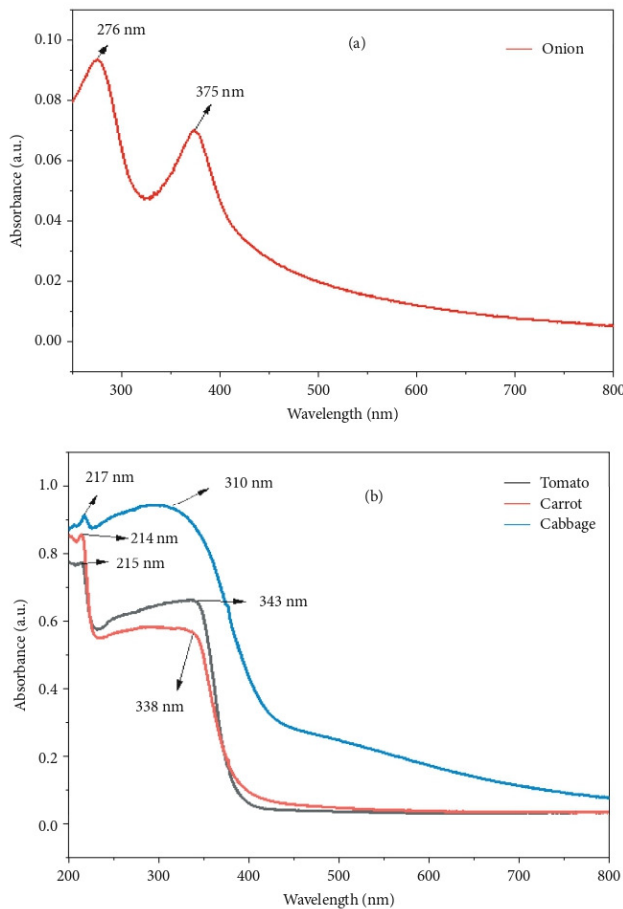


Figure 4: UV-visible absorbance spectra of the synthesized ZnO NPs' at (a) onion extraction and (b) tomato, cabbage, and carrot extraction.

The current investigation of ZnO NPs' UV-visible absorption peak is consistent with Ref. [19]. The ZnO NPs bandgap energy (E) was calculated using Planck's equation:

$$E = \frac{hc}{\lambda} \quad (2)$$

where E is the energy bandgap, h is the Planck constant, c is the speed of light, and λ is the wavelength.

The formula for converting an electron volt to a joule is $1 \text{ eV} = 1.6 \times 10^{-19} \text{ J}$ [20]. The calculated bandgap energy value for the longest wavelengths is displayed in Table 2. The electron transfers from the valences to the conduction bands are what produce ZnO's intrinsic bandgap absorption. ZnO NPs can be used in medicine for antibiotic ointments or sunburn protection because they absorb UV light [16]. ZnO NP powder can be used in metal oxide semiconductor-based systems, as evidenced by the wide range of energy bandgaps found in the 3–4 eV range [19].

Table 2: Energy bandgap of the ZnO NPs that were extracted from tomato, onion, cabbage, and carrot.

Extracted sample	Maximum wavelength	Energy bandgap
Onion	375nm	3.31 eV
Cabbage	310nm	4.01 eV
Carrot	338nm	3.68 eV
Tomato	343nm	3.62 eV

The following formula was used to determine the fill factor for dye-sensitive solar cells in order to characterize the extracted ZnO NPs:

$$ff = \frac{J_{\max} \times V_{\max}}{J_{sc} \times V_{oc}} \quad (3)$$

where J_{\max} , V_{\max} , J_{sc} , and V_{oc} stand for the voltage and current density at the peak power point, the open-circuit voltage (V_{oc}), and the small current density (J_{sc}) of a measured current at 0 V, respectively [21]. The energy conversion efficiency (n), or the ratio of maximum power (p_{\max}) to electrical input power (p_{in}), is computed as follows:

$$n = \frac{ff \times V_{oc} \times J_{sc}}{s \times p_{in}} \quad (4)$$

where s is the area of dye-sensitive solar cell [22].

At different light intensities (a , b), the electrical density (j - v) curve of a dye-sensitive solar module based on ZnO NPs is displayed in Figure 1. Equations (3) and (4) were used to extract DSSC variables from the j - v curves, including open voltage (V_{oc}), shorter-circuit current density (J_{sc}), fill factor (ff), and efficiency (n). The calculated values for the DSSC parameters [23–33] are displayed in Table 3.

It was found that the ZnO-based DSSC performed n % quite well when compared to studies with similar ZnO NPs design in the literature [22]. It has been shown that the length of time ZnO NPs are submerged together in sensitizing dye has a significant impact on the solar cell characteristics of the ZnO-based DSSC [34]. The produced ZnO-based DSSC demonstrated superior performance in a shorter sinking time [35–44] in comparison to similar studies [12–15]. The dye molecules that have been adsorbed onto the ZnO surface can also articulate the improved performance and higher absorption brought about by the greater quantity. The use of ZnO NPs in photovoltaics appears to have long-term potential due to the method's simplicity and the ease with which the specimens can be produced. It was found that the current density was significantly lower. The most important factor defining the system's overall performance limit is the photocurrent. When the particle dimension approaches that of a nanoscale, surface

energy rises and parental compounds behave differently because to their large surface area [23, 24, 34]. The ZnO NPs were synthesized with average crystallite sizes between 15 and 20 nm. We can therefore expect significant photochemical properties. A low charge collection efficiency, low injection performance, reflection or dispersion, and low hardness factor can all lead to a low [16–18].

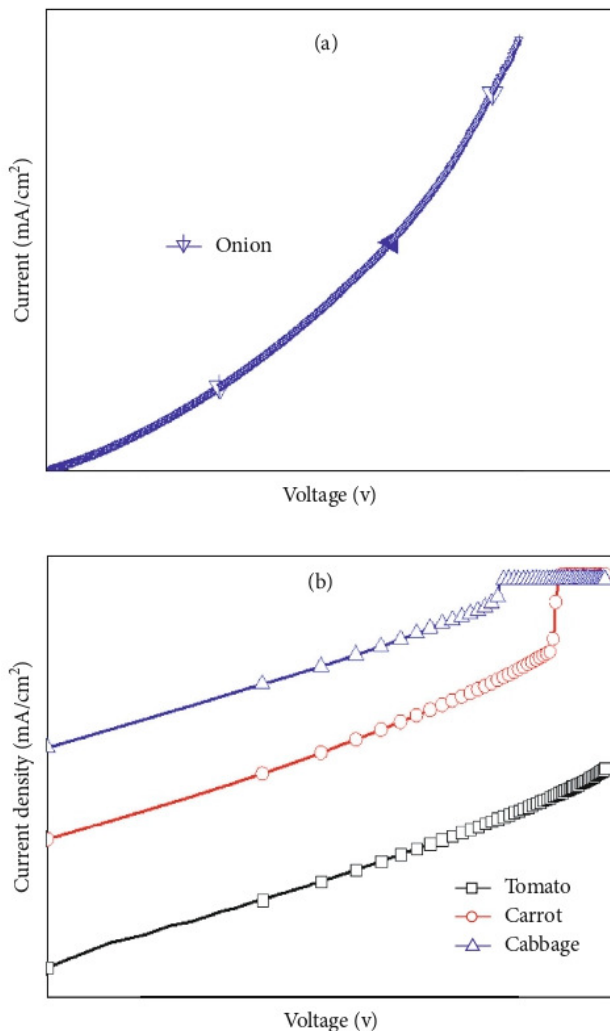


Figure 5: Green synthesized ZnO NPs' current vs. voltage curves using (a) onion extract and (b) extracts of tomatoes, cabbage, and carrots.

Table 3: Performance metric of the DSSC using the ZnO NPs that were extracted using green synthesis techniques.

Extracted sample	J_{sc} ($A\ cm^{-2}$)	V_{oc} (V)	J_{max} ($A\ cm^{-2}$)	V_{max} (V)	ff	N (%)
Onion	6.22×10^{-5}	0.38	3.20×10^{-5}	0.26	0.38	0.005
Cabbage	8.43×10^{-5}	0.22	4.21×10^{-5}	0.19	0.34	0.006
Carrot	2.99×10^{-4}	0.37	3.01×10^{-4}	0.30	0.70	0.080
Tomato	6.01×10^{-4}	0.36	0.40×10^{-4}	0.28	0.61	0.122

The output of the short circuit voltage increased gradually to levels close to saturation as the light intensity increased. The linear increase in J_{sc} was associated with higher photogenerated excitons [20–22, 34, 45]. Consequently, higher electron densities were transferred to ZnO at higher light intensities. Table 3 demonstrates that while applied light density increased, so did n and J_{sc} values. An increase in light

intensity leads to an improvement in charge generation. ZnO-based DSSC materials had previously shown similar results [19, 20, 45]. As illustrated in Figure 5, our results demonstrate that transport, injection, and recombination mechanisms are unaffected by light intensity increases up to $100\ mWcm^{-2}$.

4. Conclusions

Using a straightforward and environmentally friendly vegetable-mediated green synthesis technique, ZnO NPs were fully extracted from tomato, onion, cabbage, and carrot fruit. UV-visible spectroscopy, FTIR, XRD, and SEM were used to characterize the synthesized nanopowders. The XDR results showed that the synthesized ZnO NPs had crystal structures with particle sizes. The synthesized ZnO NPs had a single-phase hexagonal geometry with mean particle sizes of 17 nm, 18 nm, 24 nm, and 15 nm, in accordance with Scherrer's equation. The SEM results showed a little aggregation of the isolated nanoparticles. The vegetable retrieving itself would function as a capping agent or a reducing agent, depending on the circumstance, but extract capping agents were not used to reduce the clustering because they are toxic. Therefore, compared to traditional methods of synthesizing ZnO NPs, the green synthesis technique is more economical and ecologically benign. Using current density-voltage behavior under the impact of artificial sunshine, the performance of the dye-sensitive solar cell based on ZnO NPs was examined. The ZnO NP UV-visible spectroscopy showed a strong surface plasmon resonance absorption spike. The performance of the generated DSSC was improved as a result of a notable increase in dye molecule absorption on the ZnO NPs surface. Therefore, using the environmentally friendly ZnO NPs to develop dye-sensitive solar cells is an easy and promising approach for the welfare of the future. In addition to being an effective antibiotic substitute, ZnO NPs can be employed as smart weapons against a variety of drug-resistant bacteria.

References

- [1] H. Ahmad, K. Venugopal, K. Rajagopal et al., Green synthesis and characterization of zinc oxide nanoparticles using Eucalyptus globules and their fungicidal ability against pathogenic fungi of apple orchards, *Biomolecules* **10** (2020) 425.
- [2] O.J. Nava, C.A. Soto-Robles, C.M. Gómez-Gutiérrez et al., Fruit peel extract mediated green synthesis of zinc oxide nanoparticles, *J. Mol. Stru.* **1147** (2017) 1–6.
- [3] S. Thakur, M. Shandilya, G. Guleria, Appraisalment of antimicrobial zinc oxide nanoparticles through Cannabis *Jatropha curcusa* *Alovera* and *Tinosporacordifolia* leaves by green synthesis process, *J. Env. Chem. Eng.* **9** (2021) 104882.
- [4] S. Faisal, H. Jan, S.A. Shah et al., Green synthesis of zinc oxide (ZnO) nanoparticles using aqueous fruit extracts of *Myristica fragrans*: their characterizations and biological and environmental applications, *ACS Omega* **30** (2021) 9709–9722.
- [5] L.A. Kolahalam, K.R. Prasad, P.M. Krishna, N. Supraja, *Saussurea lappa* plant rhizome extract-based zinc oxide nanoparticles: synthesis, characterization and its antibacterial, antifungal activities and cytotoxic studies against Chinese Hamster Ovary (CHO) cell lines, *Heliyon* **7** (2021) e07265.
- [6] K.M. Ezealisiji, X. Siwe-Noundou, B. Maduelosi, N. Nwachukwu, R.W.M. Krause, Green synthesis of zinc oxide nanoparticles using *Solanum torvum* (L) leaf extract and evaluation of the toxicological profile of the ZnO nanoparticles–hydrogel composite in Wistar albino rats, *Int. Nano Lett.* **9** (2019) 99–107.

- [7] B. Bekele, L.T. Jule, A. Saka, The effects of annealing temperature on size, shape, structure and optical properties of synthesized zinc oxide nanoparticles by sol-gel methods, *Digest J. Nanomat. Biostr.* **16** (2021) 2.
- [8] L.T. Jule, R. Krishnaraj, B. Bekele, A. Saka, N. Nagaprasad, Experimental investigation on the impacts of annealing temperatures on titanium dioxide nanoparticles structure, size and optical properties synthesized through sol-gel methods, *Mater. Today: Proc.* **45** (2021) 5752–5758.
- [9] A. Belay, B. Bekele, and A.C. Reddy, Effects of temperature and polyvinyl alcohol concentrations in the synthesis of zinc oxide nanoparticles, *Digest J. Nanomat. Biostr.* **14** (2019) 1.
- [10] Q. Tang, H. Xia, W. Liang, X. Huo, X. Wei, Synthesis and characterization of zinc oxide nanoparticles from *Morus nigra* and its anticancer activity of AGS gastric cancer cells, *J. Photochem. Photobiol. B: Biology* **202** (2020) 111698.
- [11] D. Rehana, D. Mahendiran, R.S. Kumar, A.K. Rahiman, Evaluation of antioxidant and anticancer activity of copper oxide nanoparticles synthesized using medicinally important plant extracts, *Biomed. Pharmacot.* **89** (2017) 1067–1077.
- [12] K. Ali, S. Dwivedi, A. Azam et al., Aloe vera extract functionalized zinc oxide nanoparticles as nanoantibiotics against multi-drug resistant clinical bacterial isolates, *J. Colloid Interface Sci.* **472** (2016) 145–156.
- [13] G. Pal, P. Rai, and A. Pandey, Green synthesis of nanoparticles: a greener approach for a cleaner future, *Green Synt. Charact. Appl. Nanopart.* **548** (2019) 1–26.
- [14] S. Sarkar, R. Sarkar, Synthesis, characterization and tribological study of zinc oxide nanoparticles, *Mater. Today: Proc.* **44** (2021) 3606–3612.
- [15] R. Verma, S. Pathak, A.K. Srivastava, S. Prawer, S. Tomljenovic-Hanic, ZnO nanomaterials: green synthesis, toxicity evaluation and new insights in biomedical applications, *J. Alloys Comp.* **876** (2021) 160175.
- [16] S.C. Ezike, C.N. Hyelnasinyi, M.A. Salawu, J.F. Wansah, A.N. Ossai, N.N. Agu, Synergistic effect of chlorophyll and anthocyanin co-sensitizers in TiO₂-based dye-sensitized solar cells, *Surfaces and Interfaces* **22** (2021) 100882.
- [17] B. Sahin, S. Soylu, M. Kara, M. Turkmen, R. Aydin, H. Cetin, Superior antibacterial activity against seed-borne plant bacterial disease agents and enhanced physical properties of novel green synthesized nanostructured ZnO using *Thymra spicata* plant extract, *Ceram. Int.* **47** (2021) 341–350.
- [18] M. Amde, Z.Q. Tan, R. Liu, J.F. Liu, Nanofluid of zinc oxide nanoparticles in ionic liquid for single drop liquid microextraction of fungicides in environmental waters prior to high performance liquid chromatographic analysis, *J. Chromat. A* **1395** (2015) 7–15.
- [19] S. Alamdari, M. Sasani Ghamsari, C. Lee et al., Preparation and characterization of zinc oxide nanoparticles using leaf extract of *Sambucus ebulus*, *Appl. Sci.* **10** (2020) 3620.
- [20] A.T. Babu, R. Antony, Green synthesis of silver doped nano metal oxides of zinc & copper for antibacterial properties, adsorption, catalytic hydrogenation & photo degradation of aromatics, *J. Environ. Chem. Eng.* **7** (2019) 102840.
- [21] A. Ali, S. Ambreen, Q. Maqbool et al., Zinc impregnated cellulose nanocomposites: synthesis, characterization and applications, *J. Phys. Chem. Solids* **98** (2016) 174–182.
- [22] D. Ayodhya, G. Veerabhadram, One-pot green synthesis, characterization, photocatalytic, sensing and antimicrobial studies of *Calotropis gigantea* leaf extract capped CdS NPs, *Mater. Sci. Eng.: B* **225** (2017) 33–44.
- [23] M.A. Ansari, S.M.M. Asiri, Green synthesis, antimicrobial, antibiofilm and antitumor activities of super paramagnetic γ -Fe₂O₃ NPs and their molecular docking study with cell wall mannoproteins and peptidoglycan, *Int. J. Biol. Macromol.* **171** (2021) 44–58.
- [24] M. Faizan, J.A. Bhat, C. Chen et al., Zinc oxide nanoparticles (ZnO-NPs) induce salt tolerance by improving the antioxidant system and photosynthetic machinery in tomato, *Plant Physiol. Biochem.* **161** (2021) 122–130.
- [25] L. Tesfaye Jule, K. Ramaswamy, N. Nagaprasad, V. Shanmugam, V. Vignesh, Design and analysis of serial drilled hole in composite material, *Mater. Today: Proc.* **45** (2021) 5759–5763.
- [26] T. Amuthan, N. Nagaprasad, R. Krishnaraj, V. Narasimharaj, B. Stalin, V. Vignesh, Experimental study of mechanical properties of AA6061 and AA7075 alloy joints using friction stir welding, *Mater. Today: Proc.* **47** (2021) 4330–4335.
- [27] S. Abel, L. Tesfaye, B. Bekele, N. Nagaprasad, R. Krishnaraj, Studying the effect of metallic precursor concentration on the structural, optical, and morphological properties of zinc sulfide thin films in photovoltaic cell applications, *Adv. Mater. Sci. Eng.* **2021** (2021) 7443664.
- [28] L. Tesfaye, B. Bekele, A. Saka, N. Nagaprasad, K. Sivaramasundaram, R. Krishnaraj, Investigating spectroscopic and structural properties of Cr doped TiO₂ NPs synthesized through sol gel deposition technique, *Tierärztliche Praxis* **41** (2021) 860–872.
- [29] E.K. Subramaniam, M. Sakthivel, K. Kanthavel, R. Krishnaraj, M.G. Deepan Marudachalam, R. Palani, Overall resource effectiveness, cycle time reduction & capacity improvements, *Int. J. Sci. Eng. Res.* **2** (2011) 1–5.
- [30] R. Sathiyamoorthy, R. Krishnaraj, Optimization of cellular layout under dynamic demand environment by simulated annealing, *Int. J. Sci. Eng. Res.* **3** (2012) 1–7.
- [31] V.M.M. Thilak, R. Krishnaraj, M. Sakthivel, K. Kanthavel, M. Marudachalam, R. Palani, Transient thermal and structural analysis of the rotor disc of disc brake, *Int. J. Sci. Eng. Res.* **2** (2011) 2–5.
- [32] S. Varatharajan, R. Krishnaraj, M. Sakthivel, K. Kanthavel, M.G. Deepan Marudachalam, R. Palani, Design and analysis of single disc machine top and bottom cover, *Int. J. Sci. Eng. Res.* **2** (2011) 1–6.
- [33] C.M. Balamurugan, R. Krishnaraj, M. Sakthivel, K. Kanthavel, D. Marudachalam, R. Palani, Computer aided modeling and optimization of crankshaft, *Int. J. Sci. Eng. Res.* **2** (2011) 2–7.
- [34] T. Zahra, K.S. Ahmad, C. Zequine et al., Electro-catalyst [ZrO₂/ZnO/PdO]-NPs green functionalization: fabrication, characterization and water splitting potential assessment, *Int. J. Hydrogen Energy* **46** (2021) 19347–19362.
- [35] M. Vyshakh, R.K. Raj, A.P. Sayooj, M. Afzal, Experimental investigation on aluminium gravity die casting, *Int. J. Appl. Envir. Sci.* **9** (2014) 213–222.
- [36] M. Deepu, R.K. Raj, D. Karthik, N.M. Binoj, Cycle time optimization of rubber floor mat die, *Int. J. Appl. Envir. Sci.* **9** (2014) 229–237.
- [37] V.S. Arun, R. Krishnaraj, M.N. Rohit, V. Mohan, Optimising rejection rate of laser diamond sawing using Taguchi method, *Int. J. Appl. Envir. Sci.* **9** (2014) 223–228.
- [38] R. Krishnaraj, Investigation on the effect of thermo physical properties on heat and mass transfer–review, *Int. J. Appl. Envir.*

- Sci.* **9** (2014) 1893–1900.
- [39] C.N. Anil Kumar, R. Krishnaraj, M. Sakthivel, M. Arularasu, Implementation of safety education program for material handling equipment in construction sites and its effectiveness analysis using T-test, *Int. J. Appl. Envir. Sci.* **8** (2013) 1961–1969.
- [40] L.T. Jule, R. Krishnaraj, N. Nagaprasad, B. Stalin, V. Vignesh, T. Amuthan, Evaluate the structural and thermal analysis of solid and cross drilled rotor by using finite element analysis, *Mater. Today: Proc.* **47** (2021) 4686 - 4691.
- [41] B. Kassa, J. Leta Tesfaye, B. Bulcha et al., Effect of manganese ions on spectroscopic and insulating properties of alumino phosphate glasses, *Adv. Mater. Sci. Eng.* **2021** (2021) 6253069.
- [42] N. Nagaprasad, B. Stalin, V. Vignesh, M. Ravichandran, N. Rajini, O. Ismail, Effect of cellulosic filler loading on mechanical and thermal properties of date palm seed/vinyl ester composites, *Int. J. Biol. Macromol.* **147** (2020) 53–66.
- [43] N. Nagaprasad, B. Stalin, V. Vignesh, M. Ravichandran, N. Rajini, O. Ismail, Applicability of cellulosic-based Polyalthia longigolia seed filler reinforced vinyl ester biocomposites on tribological performance, *Polymer Composites* **42** (2020) 791–804.
- [44] B. Stalin, N. Nagaprasad, V. Vignesh, M. Ravichandran, Evaluation of mechanical and thermal properties of tamarind seed filler reinforced vinyl ester composites, *J. Vinyl Add. Technol.* **25** (2019) E114–E128.
- [45] Z. Moradi Alvand, H.R. Rajabi, A. Mirzaei, A. Masoumiasl, H. Sadatfaraji, Rapid and green synthesis of cadmium telluride quantum dots with low toxicity based on a plantmediated approach after microwave and ultrasonic assisted extraction: synthesis, characterization, biological potentials and comparison study, *Mater. Sci. Eng.: C* **98** (2019) 535–544.

Publisher's Note: Research Plateau Publishers stays neutral with regard to jurisdictional claims in published maps and institutional affiliations.